

# Critical behaviour in the nonlinear elastic response of hydrogels

M. Dennison<sup>1,3</sup>, M. Jaspers<sup>2</sup>, P.H.J. Kouwer<sup>2</sup>, C. Storm<sup>3</sup>, A.E. Rowan<sup>2</sup>, and F.C. MacKintosh<sup>1</sup>

<sup>1</sup>*Department of Physics and Astronomy, Vrije Universiteit, 1081-HV Amsterdam, The Netherlands*

<sup>2</sup>*Radboud University Nijmegen, Institute for Molecules and Materials,*

*Department of Molecular Materials, 6525-AJ Nijmegen, The Netherlands and*

<sup>3</sup>*Department of Applied Physics and Institute for Complex Molecular Systems, Eindhoven University of Technology, 5600-MB Eindhoven, The Netherlands*

(Dated: August 29, 2018)

In this paper we study the elastic response of synthetic hydrogels to an applied shear stress. The hydrogels studied here have previously been shown to mimic the behaviour of biopolymer networks when they are sufficiently far above the gel point. We show that near the gel point they exhibit an elastic response that is consistent with the predicted critical behaviour of networks near or below the isostatic point of marginal stability. This point separates rigid and floppy states, distinguished by the presence or absence of finite linear elastic moduli. Recent theoretical work has also focused on the response of such networks to finite or large deformations, both near and below the isostatic point. Despite this interest, experimental evidence for the existence of criticality in such networks has been lacking. Using computer simulations, we identify critical signatures in the mechanical response of sub-isostatic networks as a function of applied shear stress. We also present experimental evidence consistent with these predictions. Furthermore, our results show the existence of two distinct critical regimes, one of which arises from the nonlinear stretch response of semi-flexible polymers.

## I. INTRODUCTION

Highly responsive, or ‘smart’ materials are abundant in Nature; individual cells, for instance, can adapt their mechanical properties to the local surroundings by small changes in their internal structure [1]. An effective method to enhance the responsiveness of *synthetic* materials is to operate near a critical point, where small variations lead to large changes in material properties. Recent theories have suggested that fibre/polymer networks can also show critical behaviour near and below the isostatic point, the point of marginal connectivity separating rigid and floppy states [2–7]. These so called marginal networks are predicted to have many interesting and potentially useful properties that are desirable in smart materials, being highly sensitive to applied forces and fields and exhibiting an anomalously high resistance to deformation.

The isostatic point, identified 150 years ago by Maxwell [8], corresponds to the point where the number of degrees of freedom is just balanced by the number of constraints imposed by connectivity. This point of marginal stability has proven to be a rich source of inspiration for novel physics, ranging from jamming [9–11] to zero-temperature critical behaviour [2, 3] and even non-quantum topological matter [12]. However, most of this work has been theoretical, and experimental realizations of such criticality have been limited. Granular/colloidal particle packings show various signatures of criticality, including a shear modulus  $G$  that increases continuously with the distance  $\phi - \phi_c$  above the jamming volume fraction  $\phi_c$  [9–11]. Models of polymer networks and rigidity percolation can show similar critical behaviour in their linear elastic properties as a function of connectivity [13–15]. Jammed packings and spring/fiber networks are also predicted to exhibit anomalous stress-strain response

near or below the isostatic point, e.g. with power-law increase of stiffness with stress for systems with vanishing linear shear modulus [2, 6, 7, 16–18]. Such intrinsically nonlinear elasticity represents a highly responsive state of matter.

There remain important experimental challenges, however, in creating fibre or semiflexible polymer networks near a critical point, including the need to control the connectivity  $z$ , a key parameter determining both the isostatic point, as well as the nonlinear response of sub-isostatic networks to strain [7, 17]. In this paper, we study hydrogels based on synthetic semi-flexible polymers, (ethylene glycol)-substituted polyisocyanides [19, 20]. Dissolved in water and heated above the gelation temperature ( $T_{gel} \approx 19$  C), the polymers bundle together to form an intertwined network that makes up the gel. Above their gelation temperature, the network connectivity is fixed and the materials exhibit a nonlinear elastic response similar to many biopolymer systems, in which the network stiffness, defined by the differential shear modulus  $K = d\sigma/d\gamma$ , increases with shear stress  $\sigma$  as  $\sigma^{3/2}$  [21, 22]. At temperatures around  $T_{gel}$ , the network morphology is strongly correlated to the temperature, which allows a high degree of control over both the network connectivity and the properties of the individual semi-flexible filaments.

Here, we focus on the regime near and below the gel point, and demonstrate critical behaviour in the nonlinear stress response of synthetic hydrogels at low concentrations of order 0.1% volume fraction. The networks exhibit a *sub-linear* stiffening response to an applied shear stress, with  $K \propto \sigma^{\alpha < 1}$ . Using computer simulations, we show that this unexpected nonlinear elastic response is a consequence of criticality associated with the isostatic critical point. Importantly, this work implies that the influence of isostaticity can extend to network connectiv-

ities far below the isostatic critical point. Furthermore, we find that the intrinsically nonlinear stretch response of semi-flexible polymer strands in the gel gives rise to a second anomalous regime, where the networks exhibit a *super-linear* stiffening response to a shear stress distinct from the  $\sigma^{3/2}$  stiffening commonly associated with semiflexible polymer networks.

## II. RESULTS

We have performed rheology experiments and computer simulations in both linear and nonlinear elastic regimes. Full details of both the experimental and simulation methods used are given in Sec. IV. In our experimental systems we studied a range of temperatures near the gel point, while in our simulated networks we have studied systems at and below the Maxwell isostatic point. We first present results for the initial stiffening behaviour in both the experimental and simulated systems, before studying the behaviour at high shear stress.

### A. Low stress regime

#### 1. Experiments

In order to define the network rigidity we have measured the differential shear modulus, since these hydrogels are incompressible on experimentally accessible time scales, due to the presence of the solvent. The differential shear modulus is defined as  $K = \partial\sigma/\partial\gamma$ , where  $\sigma$  is the shear stress and  $\gamma$  is the shear strain. Cross-linking in our hydrogels varies with temperature, and well above the gel point ( $T \gtrsim 30^\circ\text{C}$ ), highly cross-linked gels are formed with a linear shear moduli  $G_0 \simeq 100\text{ Pa}$  [19, 20]. For  $19.5 \lesssim T \lesssim 21^\circ\text{C}$  we observe a weak initial linear elastic regime, followed by a power-law stiffening with  $K \propto \sigma^\alpha$  and  $\alpha \simeq 0.64$  (see Fig. 1(b)). The initial  $G_0$  vanishes for temperatures below  $T \simeq 19^\circ\text{C}$ , which we identify as the gel point for our system. For lower temperatures, in the range of 17 to  $19^\circ\text{C}$ , we find no apparent linear shear modulus. Instead, we observe an initial nonlinear regime with  $\alpha \simeq 0.8$  over about an order of magnitude in stress, shown in Fig. 1(c).

The observed stiffening exponents  $\alpha \simeq 0.64$  and  $0.8$  are consistent with recently predicted nonlinear elasticity of spring networks near and below the isostatic, or *marginal*, point [2, 4, 23]. Near marginal stability, a variety of critical behaviours are predicted, including a sublinear power law dependence on various stabilizing fields, such as stress [2, 4], thermal fluctuations [5, 23] and bending rigidity [3]. A simple mean-field argument suggests the appearance of  $K \sim \sigma^\alpha$  with critical stiffening exponent  $\alpha \simeq 1/2$ : in a marginal network, the linear shear modulus vanishes but any finite stress stabilizes the network, such that the modulus increases with strain  $\gamma$  as  $|\gamma|$ , resulting in  $\sigma \sim \gamma^2$  and  $d\sigma/d\gamma \sim \sigma^{1/2}$  [2, 24].

Thus, an approximate square-root dependence of  $K$  on stress is expected near the critical, or marginal, state, indicated by  $\alpha \simeq 1/2$  in the schematic phase diagram in Fig. 2. The exponent  $\alpha \simeq 1/2$  is not, however, universal. While it is present in triangular-lattice based networks [3–5] and random-bond networks [25], for square-lattice

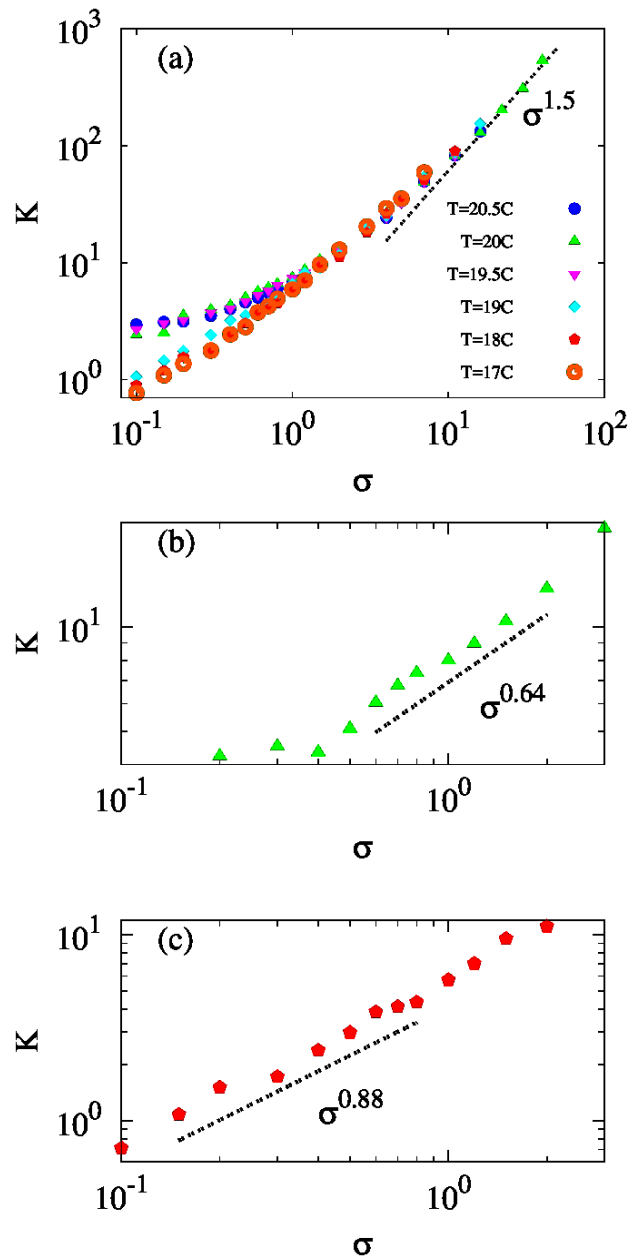


FIG. 1. (a) Differential shear modulus  $K = \partial\sigma/\partial\gamma$ , where  $\gamma$  is the shear strain, against shear stress  $\sigma$  for hydrogels at temperatures ranging from  $T = 17^\circ\text{C}$  to  $20.5^\circ\text{C}$ . The lines indicate power-law dependencies of  $K$  vs  $\sigma$ . (b) The same data, focusing on the initial sublinear scaling regimes for  $T = 20^\circ\text{C}$ . (c) The same data, focusing on the initial sublinear scaling regimes for  $T = 18^\circ\text{C}$ . All axes are in units of Pa.

based networks stiffening with an exponent  $\alpha \simeq 2/3$  has been found [23]. As we shall show, the critical stiffening of networks to an applied shear stress can be dependent on the network topology, with different critical exponents found for different initial topologies. This indicates that in experimental systems such as ours, where properties such as the degree of cross-linking and mean cross-link separation can vary greatly with the temperature, the critical stiffening exponent may not be universal.

## 2. Simulations

In order to understand our experimental observations, we performed Monte Carlo simulations on both 2D and 3D lattice-based networks. In our simulation model, we initially use Hookean springs as the model filaments. Each segment of the filament will resist stretching and

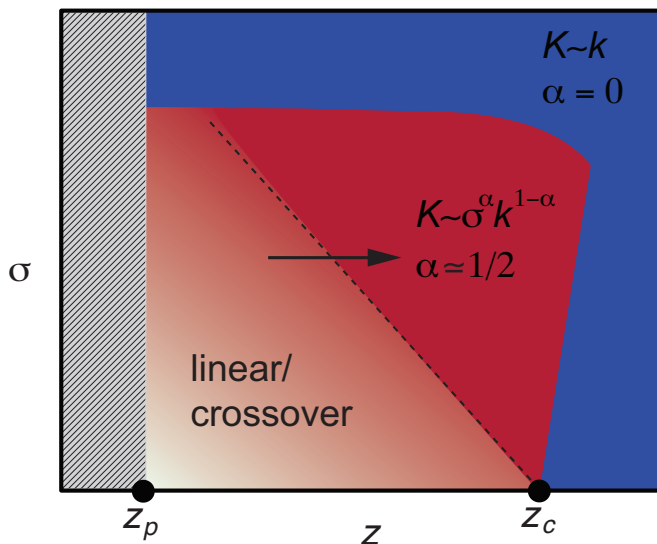


FIG. 2. Schematic phase diagram of the various regimes of network response as a function of connectivity  $z$  (average coordination of network nodes) and stress  $\sigma$ . Here,  $z_c$  is the critical connectivity, above which a purely Hookean network becomes mechanically rigid at zero temperature and stress, while  $z_p$  is the percolation point. The exponent  $\alpha$  indicates different regimes of stress dependence, characterized by network stiffness  $K \sim \sigma^\alpha k^{1-\alpha}$ , where  $k$  is the spring constant. The region labelled ‘Linear / Cross-over’ is the regime where we find sub-isostatic networks exhibit an initial linear response followed by a cross-over as they enter the critical regime. The critical regime, governed by the isostatic point, where  $\alpha$  is approximately given by the mean-field value of  $1/2$ , is indicated by the orange central triangle. In this region,  $\alpha$  is directly related to the critical exponents found at  $z_c$ . Experimentally, crosslinking (and therefore  $z$ ) increases with increasing temperature, although we are not able to measure  $z$  directly in our experiments. The expected trend in  $z$  with increasing temperature is indicated by the arrow.

compression with an energy given by

$$U_s = \frac{k}{2}(\ell - \ell_0)^2, \quad (1)$$

where  $k$  is the spring constant,  $\ell$  is the length and  $\ell_0$  is the rest length. Here, in contrast to real semi-flexible polymers, the filament may stretch indefinitely and they show only a linear force vs extension, which is not expected to accurately describe our experimental system at high stress, but can describe the behaviour at low stress. The filament stiffness is controlled by the spring constant  $k$ , which is related to the ratio of the persistence length to the segment contour length  $\ell_p/\ell_0$ , see Eq. (14). Furthermore, we also include a bending energy between sequential segments along a single filament, given by

$$U_b = \frac{\kappa}{2}\theta_{ij}^2, \quad (2)$$

where  $\kappa$  is the bending coefficient and  $\theta_{ij}$  is the angle between segments  $i$  and  $j$ .

For systems at the marginal point (Fig. 3(a) and Fig. 5(a)), we find that athermal networks ( $\ell_p/\ell_0 \rightarrow \infty$  or  $k \rightarrow \infty$ ) exhibit no initial linear response to an applied shear strain  $\gamma$ . As  $\ell_p/\ell_0$  (and hence  $k$ ) decreases, thermal fluctuations give rise to a linear response regime for both marginal and submarginal networks, in which we find  $K = G_0$ . We note that this initial linear shear modulus  $G_0$  can depend on either the thermal or the bend energy, depending on which of the two energy scales dominates. In the former case  $G_0$  behaves as in Ref. [5], while in the later it would behave as in Ref. [3]. The results shown here are for  $\kappa = 0$ , although in practice we find that both the temperature and the bending rigidity only affect this initial linear regime, and not the subsequent stiffening behaviour. This linear regime is followed by an increase in  $K$  once the stress exceeds a threshold  $\sigma_0$ , giving a  $K \sim \sigma^\alpha$  dependence with  $\alpha < 1$ . For 2D networks we observe a stiffening exponent at the marginal point of  $\alpha \sim 0.55 \pm 0.02$ , found by fitting over the region indicated in Fig 3(a), while for 3D networks we find  $\alpha \sim 0.5 \pm 0.02$ , indicated in Fig 5(a). As the modulus and stress have the same units, on dimensional grounds  $K$  should show an additional dependence on another energy scale, which we find to be the spring constant, scaling as  $K \sim \sigma^\alpha k_{sp}^{1-\alpha}$  in 2D and  $K \sim \sigma^\alpha (k/\ell_0)_{sp}^{1-\alpha}$  in 3D. Finally, at high stresses, we see that  $K$  becomes invariant to  $\sigma$  and begins to scale as  $K \sim k$ , corresponding to pure stretching of the springs.

Below the marginal state, in an initially floppy regime, the dependence of  $K$  on the stabilizing field  $\sigma$  is less clear. Prior work has shown that the *critical* regime with  $\alpha \simeq 1/2$  is not limited to systems finely-tuned to the naïve isostatic connectivity  $z_c$ , but also extends to much lower connectivities when the networks are stabilized by other interactions, such as stress [4, 5, 7]. Indeed, we find that even submarginal networks exhibit the observed critical stiffening behaviour, as can be seen in Fig 4(a) and Fig 5(a), where networks with a connectivity well below  $z_c$  are taken into a regime where they

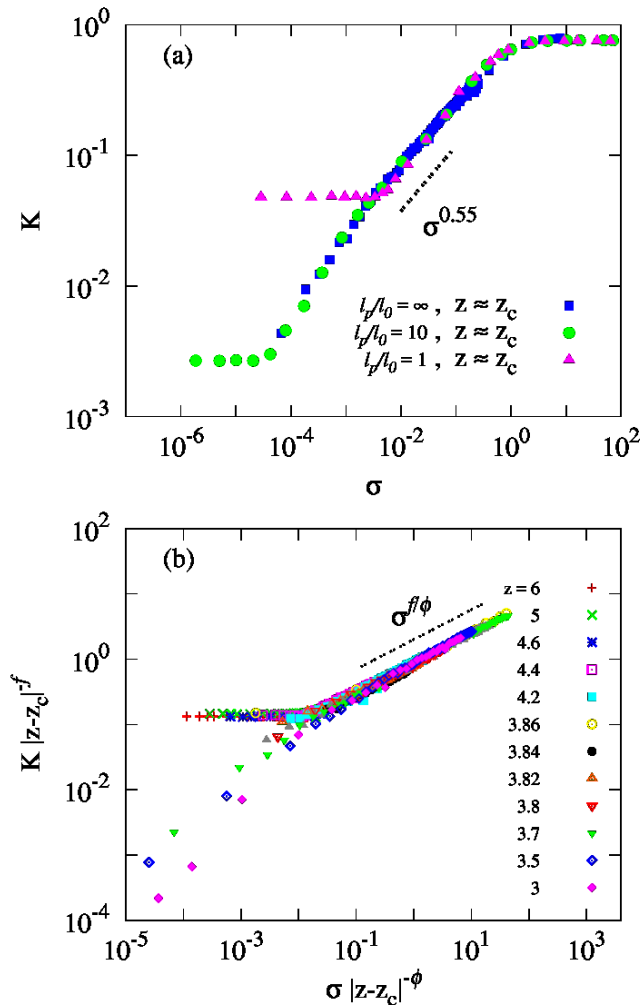


FIG. 3. (a) Differential shear modulus  $K$  vs stress  $\sigma$  for 2D Hookean spring networks with  $z = 3.85 \lesssim z_c \simeq 3.857$ .  $K$  and  $\sigma$  are in units of the spring constant  $k$ . Squares show  $l_p/l_0 = \infty$  (athermal), circles  $l_p/l_0 = 10$  and triangles  $l_p/l_0 = 1$  where  $l_p$  is the persistence length. We estimate that our experimental systems are in the range  $l_p/l_0 = 1 - 10$  [19, 20]. Dashed line shows  $K \sim \sigma^\alpha$  dependence, and indicates the region over which we fit to find  $\alpha$ . (b) Scaling collapse of the differential shear modulus  $K$ , as a function of the shear stress  $\sigma$  and the distance  $\Delta z = z - z_c$  from the critical connectivity, using the scaling ansatz given in Eq. 4. Data shown is for 2D Hookean spring networks with  $l_p/l_0 = 10$ , and with connectivities in the range 3.0 – 6.0. Here,  $f = 1.4 \pm 0.03$  and  $\phi = 2.6 \pm 0.1$ .

stiffen as  $K \sim \sigma^\alpha$  as stress is increased. Thus our experimental networks, which we expect to be submarginal with connectivity  $z \lesssim 4$  ( $z_c \sim 6$  in 3D), would be taken into a critical regime by an applied shear stress, where the network should show sublinear stiffening. We note that the size of the  $K \sim \sigma^\alpha$  stiffening regime is sensitive to the ratio  $l_p/l_0$ ; if this ratio is too small,  $G_0$  will be large enough to dominate the response, as can be seen in Fig 4(a). In Fig 4(b) we plot the stress at which sub-

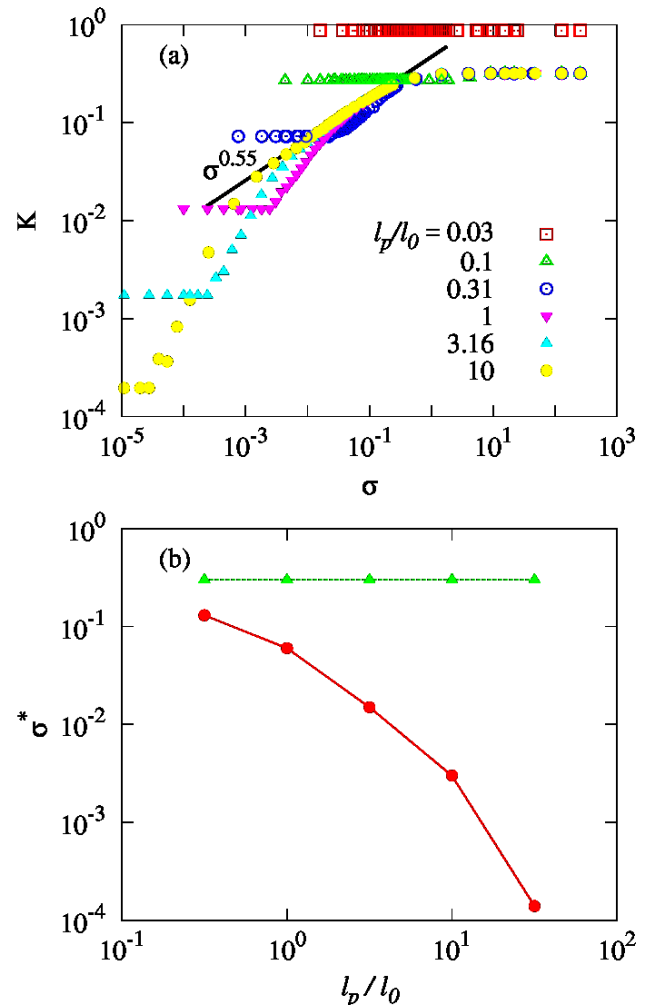


FIG. 4. (a) Differential shear modulus  $K$  vs stress  $\sigma$  for 2D Hookean spring networks with  $z = 3$ .  $K$  and  $\sigma$  are in units of the spring constant  $k$ . Legend indicates  $l_p/l_0$ , where  $l_p$  is the persistence length. We estimate that our experimental systems are in the range  $l_p/l_0 = 1 - 10$  [19, 20]. Dashed line shows  $K \sim \sigma^\alpha$  dependence in the critical regime. (b) Stress  $\sigma^*$  at which the above networks enter (red circles) and leave (green triangles) the critical regime, where we observe a  $K \sim \sigma^{0.55}$  dependence, for networks with a range of  $l_p/l_0$  values.

marginal 2D networks (with  $z = 3$ ) enter the critical regime as a function of the ratio of persistence length to segment length. As can be seen, networks with a higher value of  $l_p/l_0$  (corresponding to stiff filaments) will enter the critical regime at a much lower stress than networks with a lower value.

In order to examine if this is true critical behaviour we have calculated the non-affine fluctuations of the system, which are known to diverge at critical points in elastic networks. We first define the differential non-affinity  $\Gamma$

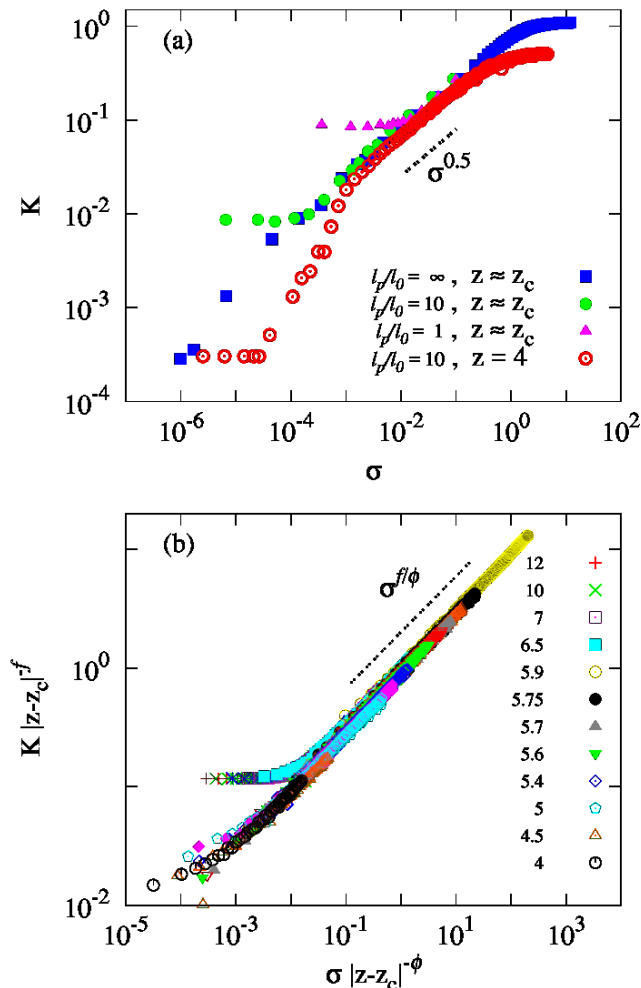


FIG. 5. (a) Main plot: Differential shear modulus  $K$  vs stress  $\sigma$  for 3D Hookean spring networks with  $z = 5.84 \lesssim z_c \simeq 5.844$  (solid symbols) and  $z = 4$  (open symbols).  $K$  and  $\sigma$  are in units of  $k/\ell_0$ , where  $k$  is the spring constant and  $\ell_0$  is the rest length of the springs (which also gives the segment contour length). Squares show  $\ell_p/\ell_0 = \infty$  (athermal), circles  $\ell_p/\ell_0 = 10$  and triangles  $\ell_p/\ell_0 = 1$  where  $\ell_p$  is the persistence length. We estimate that our experimental systems are in the range  $\ell_p/\ell_0 = 1 - 10$  [19, 20]. Dashed lines show  $K \sim \sigma^\alpha$  dependencies, and indicate the region over which we fit to find  $\alpha$ . Inset:  $K$  vs  $\sigma$  for 3D networks with  $z = 5.84 \lesssim z_c \simeq 5.844$  using semi-flexible filaments (see methods), with  $\ell_p/\ell_0 = 10$ . Both axes are in units of  $k/\ell_0$ , where here  $k$  is an effective spring constant. (b) Scaling collapse of the differential shear modulus  $K$ , as a function of the shear stress  $\sigma$  and the distance  $\Delta z = z - z_c$  from the critical connectivity, using the scaling ansatz given in Eq. 4. Data shown is for 3D Hookean spring networks with  $\ell_p/\ell_0 = 10$ , and with connectivities in the range 4.0 – 12.0. Here,  $f = 1.6 \pm 0.1$  and  $\phi = 3.2 \pm 0.1$ .

as

$$\Gamma = \frac{1}{\ell_0^2} \frac{\langle \Delta \mathbf{r}^2 \rangle}{(\Delta \gamma)^2}, \quad (3)$$

where  $\mathbf{r} = \mathbf{r}_{na} - \mathbf{r}_a$  is the non-affine contribution to the node displacement, with  $\mathbf{r}_{na}$  the position of a node and  $\mathbf{r}_a$  the position if the displacement would have been affine.  $\langle \dots \rangle$  denotes the average over all nodes. A high value of  $\Gamma$  means that the network deformation is more differentially non-affine, while a low value means it is less so.

Figure 6 shows  $\Gamma$  against the applied shear strain  $\gamma$  for networks with connectivity  $z = 3.5$  (well below the marginal point  $z_c = 3.857$ ), simulated at a range of bending rigidities  $\kappa$  (see Eq. (8)) in the athermal limit of  $\ell_p/\ell_0 \rightarrow \infty$ . We choose to plot our data against  $\gamma$  instead of  $\sigma$  as the networks will enter the critical regime at similar strains but vastly different stresses. For low bending rigidities  $\kappa$  we find that, as the strain is increased,  $\Gamma$  increases, reaching a peak at a value corresponding to the network entering the critical regime, where the differential shear modulus scales as  $K \sim \sigma^\alpha$ . Beyond this peak  $\Gamma$  decreases with increasing  $\gamma$ . This divergence of the differential non-affinity is further evidence that we are in a true critical regime. For higher values of  $\kappa$  we find that the peak value decreases, until eventually no divergence is found, indicating that in this case the bending rigidity suppresses criticality, consistent with previous work [3].

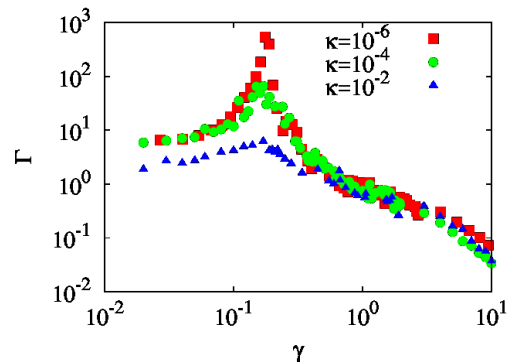


FIG. 6. Differential non-affinity  $\Gamma$  against applied shear strain  $\gamma$  for 2D Hookean spring networks with connectivity  $z = 3.5$ . Data is for various bending rigidities  $\kappa$ .

In the critical regime, the stiffening exponent  $\alpha = f/\phi$  is directly related to critical exponents  $f$  and  $\phi$  defined by

$$K = k |\Delta z|^f \mathcal{F} \left( \frac{\sigma}{k} |\Delta z|^{-\phi} \right), \quad (4)$$

which is demonstrated in Fig. 3(b) and Fig. 5(b). Such cross-over scaling has been demonstrated previously for the critical point of random resistor networks [26], fiber networks [3] and both athermal and thermal spring networks [2, 5]. Here we find  $f = 1.4 \pm 0.03$  and  $\phi = 2.6 \pm 0.1$  (with  $\alpha = 0.54$ ) for 2D networks and  $f = 1.6$  and  $\phi = 3.2$  (with  $\alpha = 0.5$ ) for 3D networks. These stiffening exponents are comparable to the values observed experimentally and close to the mean-field value of  $\alpha = 1/2$  [2]. However, as noted previously, different network topologies can exhibit different critical exponents. Random

bond networks have been shown to exhibit mean-field like stiffening with temperature  $T$  at the critical point, with  $G_0 \sim T^\alpha$  where  $\alpha = f/\phi = 1/2$  with  $f = 1$  and  $\phi = 2$ . Square lattices, which are marginal objects, stiffen with  $G_0 \sim T^\alpha$  where  $\alpha \simeq 2/3$  [23].

In order to see how systems with different topologies stiffen with an applied shear stress we have simulated a square lattice network in 2D and a simple cubic lattice in 3D, and the results are shown in Fig. 7(a), where we compare the stiffening to that of triangular (2D) and FCC (3D) lattice based networks. These networks are marginal objects, as any deformation will result in a cost in energy, and as can be seen, the network stiffens as  $K \sim \sigma^\alpha$  with  $\alpha \sim 0.66$ , distinct from the  $\alpha \sim 0.55$  found for the triangular lattice network. The same behaviour can be seen for 3d networks using a simple cubic lattice, and exhibits stiffening with  $\alpha \sim 0.66$  (Fig. 7(b)), again distinct from the  $\alpha \sim 0.5$  found for the FCC lattice network. This implies that the starting topology is important: two networks can stiffen with two different critical exponents depending on the initial topology, with the network with a higher possible local  $z$  ( $z = 12$  for an FCC lattice) have a lower critical stiffening exponent than that with a lower possible local  $z$  ( $z = 6$  for a simple cubic lattice).

## B. High stress regime

### 1. Experiments

As the stress in our experimental systems is increased beyond the initial  $K \sim \sigma^\alpha$  regime, we find a second stiffening regime, for which we define a second exponent  $\beta \simeq 1.2$ , as can be seen in Fig. 1 and more clearly in Fig. 8. This exponent is distinct from the asymptotic exponent of 1.5 observed previously for this system [19]. We hypothesize that this arises from the nonlinear spring constant of the polymers making up the network [19, 21, 22, 27, 28]. As the stress increases, these polymers stretch and enter a nonlinear regime characterized by a force-extension relation in which the force

$$f \sim 1/|1 - \epsilon|^2 \quad (5)$$

depends on the relative extension  $\epsilon$  [27, 29, 30]. This leads to an effective spring constant  $k_{\text{sp}} \propto f^{3/2}$ , where  $f \propto \sigma$  is the force on the segment. At low stresses the force-extension relation is linear  $f \sim \epsilon$ , and hence the effective spring constant is independent of stress. As we have shown from our simulation results, the network stiffness scales as  $K \sim \sigma^\alpha \times k^{1-\alpha}$  [4]. Thus, if we substitute in  $k_{\text{sp}} \propto \sigma^{3/2}$ , we predict an initial  $K \sim \sigma^\alpha$  regime at low stresses, followed by  $K \sim \sigma^\beta$  at higher stresses, where

$$\beta = 3/2 - \alpha/2. \quad (6)$$

Beyond this regime, at very high stresses, we see evidence of the  $K \sim \sigma^{1.5}$  regime expected for semi-flexible polymer networks.

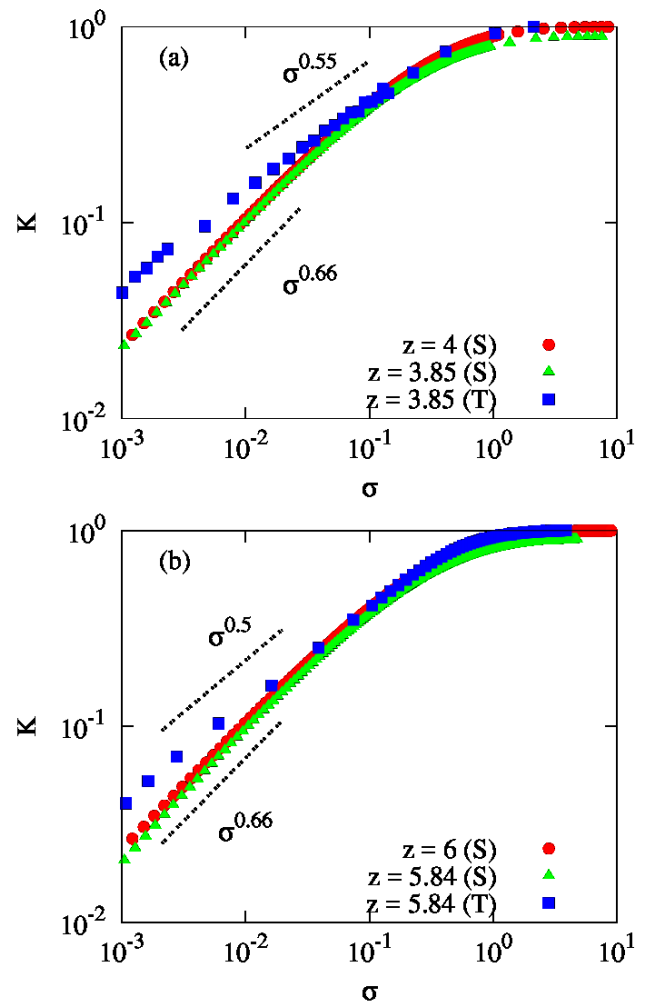


FIG. 7. (a) Differential shear modulus  $K$  vs stress  $\sigma$  for 2D Hookean spring networks using triangular lattice based networks at the marginal point  $z = 3.85 \simeq z_c$  (squares) and square lattice networks with  $z = 4$  (circles) and  $z = 3.85$  (triangles).  $K$  and  $\sigma$  are in units of the spring constant  $k$ . Dashed lines show  $K \sim \sigma^\alpha$  dependencies, and indicate the region over which we fit to find  $\alpha$ . Data for the triangular lattice system has been shifted to better show the observed stiffening. (b)  $K$  against  $\sigma$  for 3D Hookean spring networks using FCC lattice based networks at the marginal point  $z = 5.84 \simeq z_c$  (squares) and simple cubic lattice networks with  $z = 6$  (circles) and  $z = 5.84$  (triangles).  $K$  and  $\sigma$  are in units of  $k/\ell_0$ . Dashed lines show  $K \sim \sigma^\alpha$  dependencies, and indicate the region over which we fit to find  $\alpha$ . Data for the FCC lattice system has been shifted to better show the observed stiffening.

### 2. Simulations

In order to understand this intermediate regime in our experimental system, corresponding to  $1\text{Pa} \lesssim \sigma \lesssim 10\text{Pa}$  in Fig. 1 where we observed  $K \sim \sigma^\beta$ , we simulated networks using the nonlinear response of semi-flexible filaments. Full details are given in the methods section, Eq. (11) to Eq. (12). Here the filament stretch response

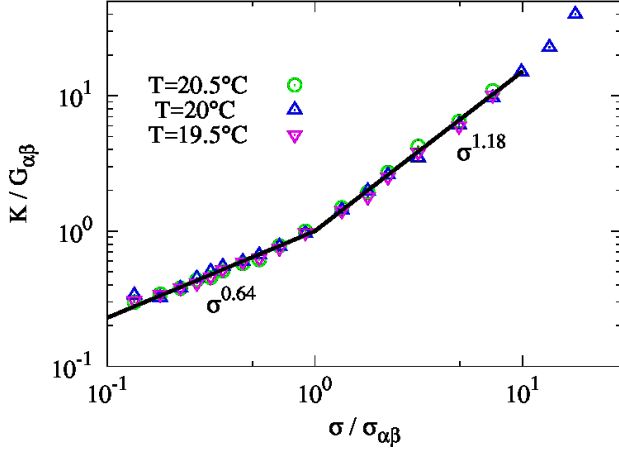


FIG. 8. Differential shear modulus  $K$  against stress  $\sigma$  measured at temperatures from  $T = 19.5$  to  $20.5^\circ$  C.  $K$  and  $\sigma$  are normalized by the empirical values  $G_{\alpha\beta}$  and  $\sigma_{\alpha\beta}$ , the differential modulus and shear stress at the crossover from the  $\alpha$  to  $\beta$  regimes. Solid lines show  $K \sim \sigma^{0.64}$  and  $K \sim \sigma^{1.18}$  dependence.

is initially linear, followed by a strong stiffening due to the pulling out of thermal bending modes. As for the Hookean spring model, the filament stiffness is controlled by the effective spring constant  $k$ , related to  $\ell_p/\ell_0$ , see Eq. (14). Our results are shown for 2D in Fig. 9(a) and 3D networks in Fig. 9(b). Following an initial regime with  $K \sim \sigma^\alpha$ , we find both  $K \sim \sigma^\beta$  and  $K \sim \sigma^{3/2}$  regimes, where  $\beta$  obeys Eq. (6). We stress that this relation holds for both 2D and 3D networks, as well as for different initial network topologies. This can be seen in Fig. 9(a), where we also show data for diluted square lattice networks, which show  $\alpha \sim 0.66$  (as in Fig. 7), and  $\beta \sim 1.17$ . These results are also consistent with the phase diagram in Fig. 2, with both  $K \sim \sigma^\alpha \times k_{sp}^{1-\alpha}$  at intermediate stress and  $K \sim k$  at high stress, where  $k \propto \sigma^{3/2}$ , consistent with known extensional properties of semi-flexible polymers [19, 21, 22, 24, 27–30]. These observations can account for our experimental results for  $1\text{Pa} \lesssim \sigma \lesssim 10\text{Pa}$ .

In Fig. 8, we show data for experimental networks at  $T = 19.5 - 20.5^\circ$  C with  $K$  (and  $\sigma$ ) scaled by the shear modulus  $G_{\alpha\beta}$  (and stress  $\sigma_{\alpha\beta}$ ) at which we observe the cross-over from  $\alpha$  to  $\beta$  regimes. Here we find excellent agreement of the data using an initial stiffening exponent  $\alpha \sim 0.64$ , followed by  $\beta \sim 1.18$  obtained from Eq. (6). In Fig. 10(a) we show the values of  $\alpha$  and  $\beta$  found for individual temperatures from 17 to  $21^\circ$  C, which again show good agreement with the relation given in Eq. (6). Importantly, the prediction (dashed line) contains no adjustable parameters. Finally, we also observe an evolution of the cross-over stress  $\sigma_{\alpha\beta}$ , which increases with increasing  $T$  (Fig. 10(c)). This is also consistent with the predicted trend with increasing  $z$ , shown in Fig. 10(b). This behaviour further indicates that the connectivity increases with the temperature, as indicated in

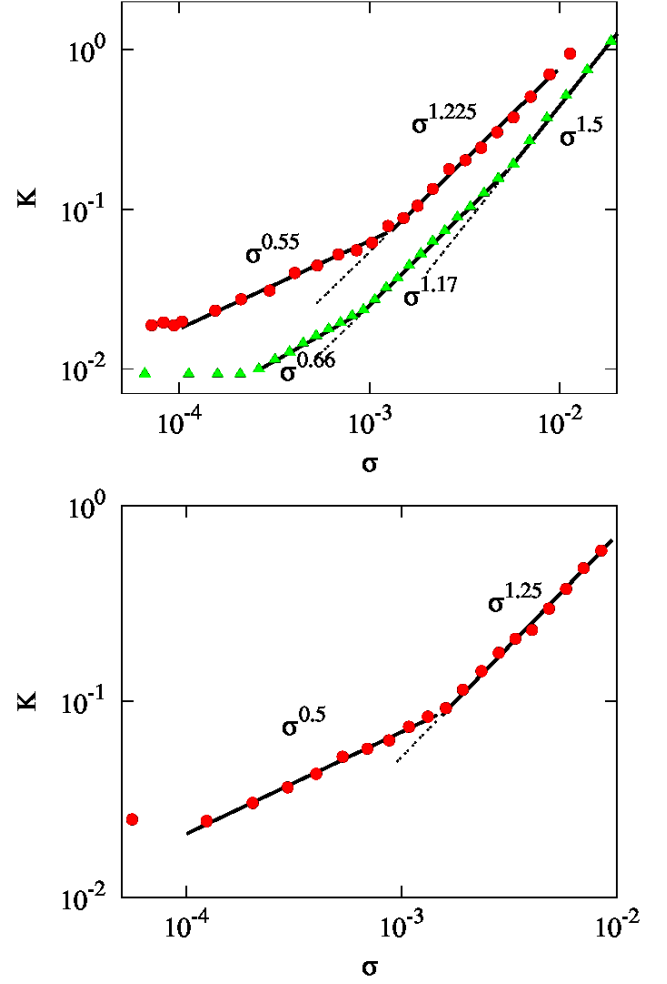


FIG. 9. (a) Differential shear modulus  $K$  vs stress  $\sigma$  for 2D networks with  $z = 3.85 \lesssim z_c \simeq 3.857$  using semi-flexible filaments (see methods), with  $\ell_p/\ell_0 = 10$ , indicated by the red circles. Both axes are in units of  $k$ , where here  $k$  is an effective spring constant, see Eq. (14). Lines show  $K \sim \sigma^\alpha$  and  $K \sim \sigma^\beta$  dependencies, and indicate the region over which we fit to find  $\alpha$  and  $\beta$ . Green triangles indicate data for a diluted square lattice network, also with  $z = 3.857$ , with the  $K \sim \sigma^\alpha$ ,  $K \sim \sigma^\beta$  and  $K \sim \sigma^{1.5}$  dependencies indicated. (b)  $K$  vs  $\sigma$  for 3D networks with  $z = 5.84 \lesssim z_c \simeq 5.844$  using semi-flexible filaments (see methods), with  $\ell_p/\ell_0 = 10$ . Both axes are in units of  $k/\ell_0$ .

the schematic phase diagram in Fig. 2 by the solid arrow, corresponding to the variation of  $z$  one would expect for increasing temperature.

### III. CONCLUSIONS

We have shown that synthetic hydrogels exhibit an elastic response consistent with predicted critical behaviour associated with isostatic and subisostatic networks. Our results show that these hydrogels stiffen sub-

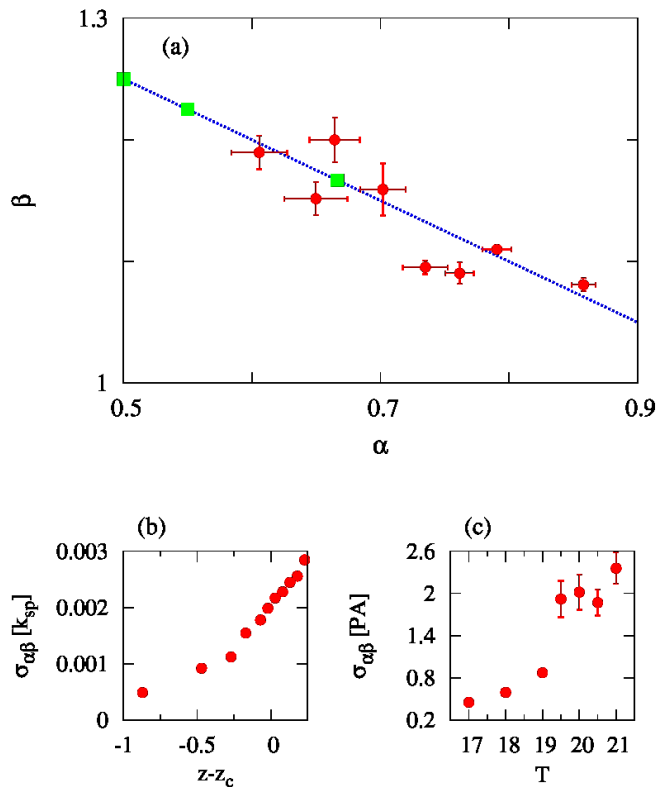


FIG. 10. (a) Values of  $\alpha$  and  $\beta$  found for individual temperatures ranging from  $T = 17$  to  $21^\circ\text{C}$ , indicated by the red circles. Line shows the relation  $\beta = 1.5 - 0.5\alpha$ , while green squares show simulation data for 2d (triangular lattice with  $\alpha \sim 0.55$  and square lattice with  $\alpha \sim 0.66$ ) and 3d ( $\alpha \sim 0.5$ ) networks. (b) Stress  $\sigma_{\alpha\beta}$  at the cross-over from the initial sub-linear  $\alpha$  stiffening regime to the second, superlinear  $\beta$  regime, against distance from the critical connectivity  $z - z_c$  for simulated 3D networks using the potential in Eqs. (11)-(12) to model the filaments. Here  $\sigma_{\alpha\beta}$  is in units of the effective spring constant  $k$  given in Eq. (13). (c)  $\sigma_{\alpha\beta}$  (given in Pa) for experimental networks, against temperature  $T$ .

linearly under an applied shear stress and exhibit a critical stiffening exponent that is consistent with that predicted theoretically and in computer simulations. Perhaps surprisingly, even networks deep into the subisostatic regime are predicted to exhibit such behaviour. This can account for our experimental results, where all the samples are expected to be in the sub-isostatic regime, corresponding to local connectivities  $z \lesssim 4 < z_c$  in 3D. This suggests that the marginal point is an important control mechanism for the elastic stability of networks in response to an applied shear stress, and our results support the proposed phase diagram in Fig. 2, indicating a very broad range over which critical control of mechanics is possible. Furthermore, both our simulation and experimental results show the existence of a second regime of critical stiffening, where the individual filaments exhibit a non-linear response to stretch deformation resulting in a superlinear stiffening regime.

This work also identifies the ratio of the persistence length to the cross-link separation,  $\ell_p/\ell_0$ , as key design parameters: this should be of the order of 0.1 – 10 to achieve critical control of network mechanics. When the polymers are too flexible, for instance, the linear shear modulus dominates the stiffening behaviour. Thus, for synthetic polymers that are usually flexible, controlled bundle formation may be important for future materials development using these principles. This work demonstrates an experimentally realizable system that exhibits mechanical critical behaviour, opening the way for further experimental studies of marginal/isostatic networks.

## ACKNOWLEDGMENTS

We acknowledge financial support from FOM/NWO (M.D, C.S, F.C.M), NRSCC (M.J, A.E.R) NWO Gravitation (A.E.R, P.H.J.K) and NanoNextNL (A.E.R, P.H.J.K). We would like to thank David Weitz for fruitful discussions and suggestions.

M.D, C.S and F.C.M designed the simulations. M.D. performed the simulations. M.J, P.H.J.K and A.E.R designed the experimental work. M.J. synthesised the polymers and carried out the mechanical tests. All authors contributed to the writing of the paper.

## IV. METHODS

### A. Experiments

Our gels were synthesized and purified following a previously described procedure [19], and an AFM image of individual polymers is shown in Fig. 11. The catalyst/monomer ratio of 1 : 2000 yielded a polymer of average molecular weight  $M_v = 400 \text{ kg mol}^{-1}$  as determined by viscometry. For gel studies, the polymer was dissolved in purified water (milliQ) by stirring for at least 24 hrs at  $4^\circ\text{C}$ . Rheology was performed, by default, with a stress-controlled rheometer (Discovery HR-1, TA Instruments) with an aluminium parallel plate geometry (40 mm diameter) and a gap of  $500 \mu\text{m}$ . Samples were inserted in the rheometer at  $5^\circ\text{C}$  (i.e. as a liquid) and gelation occurred between the setup by raising the temperature using a peltier plate. Drying of the sample was prevented by maintaining a moist atmosphere. The storage modulus in the linear regime was obtained by applying an oscillatory strain of 1% at a frequency of 1 Hz and measuring the sinusoidal stress response. The non-linear regime was probed by applying a steady pre-stress  $\sigma$  to the sample and superposing a small oscillatory stress with an amplitude of  $|\delta\sigma| < 0.1\sigma$  at a frequencies 0.1 – 10 Hz. The differential modulus was calculated from the oscillatory strain response  $\delta\gamma$ , as  $K = \partial\sigma/\partial\gamma = \delta\sigma/\delta\gamma$ . To investigate the role of the non-linear strain-field that of the parallel plate setup, we measured for selected samples the



mechanical properties in a Couette and cone and plate geometry (Fig. 12). The experimental details are as follows: Cone and plate geometry: aluminium, 40 mm diameter, cone angle  $1^\circ$ , truncation gap  $29 \mu\text{m}$ ; Couette geometry: aluminium cup and bob, cup diameter 30.41 mm, bob diameter 27.98 mm (thus a gap of 1.22 mm), bob length 42.10 mm.

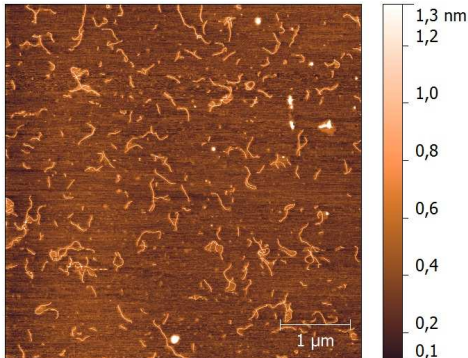


FIG. 11. AFM image of individual polymers spincoated from a 0.1 mg/mL solution of the polymer in dichloromethane on freshly cleaved Mica. The scale bar is indicated in the figure.

Although the strain field in the plate-plate geometry is not constant, the linear and non-linear mechanical properties are well represented. As an illustration, we show the (non-)linear mechanical properties at two different temperatures in three different configurations: plate-plate; cone-plate and Couette, see Fig. 12. For both temperatures, the results from either configuration are similar over the entire stress range, in line for what was observed in gels based on actin [21].

## B. Simulations

We use the Monte Carlo method to simulate two- and three-dimensional lattice-based networks. The network nodes are initially arranged on a triangular lattice in 2D and on an FCC lattice in 3D, and are allowed to fluctuate off-lattice during the simulations. Nearest neighbour nodes are connected with model filament segments to give a fully connected network with  $z = 6$  in 2D and  $z = 12$  in 3D, before random segments are removed to lower the network connectivity  $z$ .

In this work we have used two types of model filaments. The first is the Hookean spring model, which has been used in many previous studies [3–5, 31], where the stretching or compression of a filament segment  $i$  will involve a cost in energy given by

$$\mathcal{U}_s = \frac{k}{2}(\ell_i - \ell_{0,i})^2, \quad (7)$$

where  $\ell_i$  is the length and  $\ell_{0,i}$  is the contour length of segment  $i$ , and  $k$  is the spring constant. In such a model

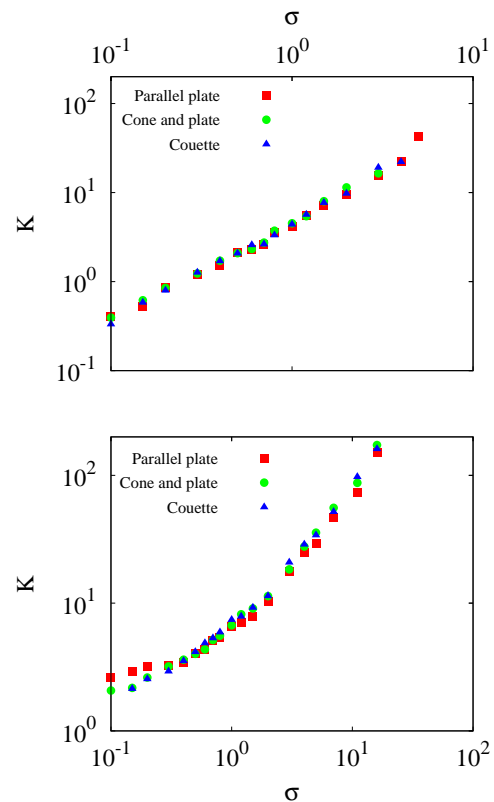


FIG. 12. Differential modulus  $K$  as a function of stress  $\sigma$  for three different geometries at (a)  $T = 17^\circ \text{C}$  (in the ‘pre-gel’ regime) and (b) at  $T = 20^\circ \text{C}$  (just above the gel point). All axes are in units of Pa.

the segments may stretch indefinitely and show only a linear force-extension for any deformation. A bending rigidity is also incorporated, where the energy cost for bending two coaxially connected springs,  $i$  and  $j$ , is given by

$$\mathcal{U}_b = \frac{\kappa}{2}\theta_{ij}^2, \quad (8)$$

where  $\kappa$  is the bending rigidity and  $\theta_{ij}$  is the angle between springs  $i$  and  $j$ .

In order to capture the non-linear response of semi-flexible polymers to stretching and compression we include a nonlinear spring to represent the known force-extension appropriate for stiff chain segments of length  $\ell_0 \lesssim \ell_p$  [24, 27, 28, 32], which can be well-approximated by a combination of the divergence in Eq. 5, together with a linear spring [21, 24, 33]. Here, we follow the approach presented in Ref. [33] and use a nonlinear potential to more accurately describe the experimental filament response [34]. This can be summarized by the force along a stretched segment which is given by

$$f = \frac{9k_B T \ell_p}{\ell_{0,i}^2} \left[ \frac{1}{(1-\epsilon)^2} - 1 - \frac{1}{3}\epsilon \right], \quad (9)$$

where  $T$  is the temperature,  $k_b$  the Boltzmann constant

and  $\epsilon_i$  is the scaled extension of filament  $i$ , given by

$$\epsilon_i = \frac{1}{6} + \frac{\ell_p \ell_i}{\ell_{0,i}^2} - \frac{\ell_p}{\ell_{0,i}}, \quad (10)$$

where  $\ell_p$  is the persistence length of the filaments. For lattice networks the contour lengths are identical for all segments. The energy due to a deformation of filament segment  $i$  is then given by

$$\frac{\mathcal{U}_s}{k_b T} = \begin{cases} -\frac{9\epsilon_i^2[5 + 6\epsilon_i]}{6\epsilon_i - 1} & \epsilon_i > 0, \\ \left| \pi^2 \epsilon_i - \frac{\pi^4}{90} (\exp[90\epsilon_i/\pi^2] - 1) \right| & \epsilon_i < 0, \end{cases} \quad (11)$$

The top line in Eq. (11) gives the energy cost for stretching, while the bottom line that for compression. In this more realistic model a bending energy is also applied to the system, which again acts on pairs of filament segments that are connected coaxially at the network nodes. The energy due to the bending of connected filaments  $i$  and  $j$  is given by [33]

$$\frac{\mathcal{U}_b}{k_b T} = \frac{\ell_p \theta_{ij}^2}{\ell_{0,i} + \ell_{0,j}}, \quad (12)$$

where  $\theta_{ij}$  is the angle between the end-to-end vectors of filament segments  $i$  and  $j$ .

The stiffness of Hookean springs is controlled by the spring constant  $k$ , while for the semi-flexible potential it is controlled by the persistence length  $\ell_p$ . These can be related through an effective spring constant given by

$$k = \frac{90k_b T \ell_p^2}{\ell_0^4}, \quad (13)$$

or alternatively by the reduced persistence length

$$\ell'_p = \frac{\ell_p}{\ell_0} = \sqrt{\frac{k \ell_0^2}{90k_b T}} \quad (14)$$

We note that for small deformations of a segment the energy cost is the same for both the semi-flexible and the Hookean spring potentials when the spring constants (or reduced persistence lengths) are equal.

The networks are then sheared using Lees-Edwards boundary conditions [35]. After applying a shear strain  $\gamma$  to the system, we calculate the shear stress  $\sigma$  and differential modulus  $K$  as described in Refs. [5, 36].

- 
- [1] P. A. Janmey and D. A. Weitz, *Trends in biochemical sciences*, 2004, **29**, 364–370.
- [2] M. Wyart, H. Liang, A. Kabla and L. Mahadevan, *Phys. Rev. Lett.*, 2008, **101**, 215501.
- [3] C. P. Broedersz, T. C. Lubensky, X. Mao and F. C. MacKintosh, *Nature Physics*, 2011, **7**, 983.
- [4] M. Sheinman, C. P. Broedersz and F. C. MacKintosh, *Phys. Rev. Lett.*, 2012, **109**, 238101.
- [5] M. Dennison, M. Sheinman, C. Storm and F. C. MacKintosh, *Phys. Rev. Lett.*, 2013, **111**, 095503.
- [6] J. Feng, H. Levine, X. Mao and L. M. Sander, *Soft Matter* DOI:10.1039/C5SM01856K (2016).
- [7] A. Sharma, A. J. Licup, K. A. Jansen, R. Rens, M. Sheinman, G. H. Koenderink and F. C. MacKintosh, *Nature Physics* DOI: 10.1038/NPHYS3628 (2016).
- [8] J. C. Maxwell, *Philos. Mag.*, 1864, **27**, 297.
- [9] M. E. Cates, J. P. Wittmer, J.-P. Bouchaud and P. Claudin, *Phys. Rev. Lett.*, **81**, 1841.
- [10] A. J. Liu and S. R. Nagel, *Annu. Rev. Condens. Matter Phys.*, 2010, **1**, 347.
- [11] M. van Hecke, *J. Phys.: Condens. Matter*, 2010, **22**, 033101.
- [12] C. L. Kane and T. C. Lubensky, *Nature Physics*, 2013, **10**, 39.
- [13] R. G. Larson, *The Structure and Rheology of Complex Fluids*, Oxford University Press, 1998.
- [14] S. Feng and P. N. Sen, *Phys. Rev. Lett.*, 1984, **52**, 216.
- [15] D. J. Jacobs and M. F. Thorpe, *Phys. Rev. E*, 1996, **53**, 3682.
- [16] S. Alexander, *Phys. Rep.*, 1998, **296**, 65.
- [17] M. Sheinman, C. P. Broedersz and F. C. MacKintosh, *Phys. Rev. E*, 2012, **85**, 021801.
- [18] M. S. van Deen, J. Simon, Z. Zeravcic, S. Dagois-Bohy, B. P. Tighe and M. van Hecke, *Phys. Rev. E*, 2014, **90**, 020202.
- [19] P. H. J. Kouwer, M. Koepf, V. A. A. Le Sage, M. Jaspers, A. M. van Buul, Z. H. Eksteen-Akeroyd, T. Woltinge, E. Schwartz, H. J. Kitto, R. Hoogenboom, S. J. Picken, R. J. M. Nolte, E. Mendes and A. E. Rowan, *Nature*, 2013, **493**, 651.
- [20] M. Jaspers, M. Dennison, M. F. Mabesoone, F. C. MacKintosh, A. E. Rowan and P. H. Kouwer, *Nature communications*, 2014, **5**, year.
- [21] M. L. Gardel, J. H. Shin, F. C. MacKintosh, L. Mahadevan, P. Matsudaira and D. A. Weitz, *Science*, 2004, **304**, 1301.
- [22] Y. C. Lin, N. Y. Yao, C. P. Broedersz, H. Herrmann, F. C. MacKintosh and D. A. Weitz, *Phys. Rev. Lett*, 2010, **104**, 058101.
- [23] X. Mao, A. Souslov, C. I. Mendoza and T. C. Lubensky, *Nature Communications*, 2015, **6**, 5968.
- [24] C. P. Broedersz and F. C. MacKintosh, *Rev. Mod. Phys.*, 2014, **86**, 995.
- [25] M. C. Wigbers, F. C. MacKintosh and M. Dennison, *Phys. Rev. E*, 2015, **92**, 042145.
- [26] J. Straley, *J. Phys. C: Solid State Phys.*, 1976, **9**, 783.
- [27] F. C. MacKintosh, J. Kas and P. Janmey, *Phys. Rev. Lett.*, 1995, **75**, 4425.
- [28] C. Storm, J. J. Pastore, F. C. MacKintosh, T. C. Lubensky and P. A. Janmey, *Nature*, 2005, **435**, 191.
- [29] M. Fixman and J. Kovac, *The Journal of Chemical Physics*, 1973, **58**, 1564.
- [30] J. F. Marko and E. D. Siggia, *Macromolecules*, 1995, **28**, 8759–8770.
- [31] C. P. Broedersz, M. Sheinman and F. C. MacKintosh, *Phys. Rev. Lett.*, 2012, **108**, 078102.

- [32] T. Odijk, *Macromolecules*, 1995, **28**, 7016–7018.
- [33] E. M. Huisman, C. Storm and G. T. Barkema, *Phys. Rev. E*, 2008, **78**, 051801.
- [34] A. M. van Buul, E. Schwartz, P. Brocorens, M. Koepf, D. Beljonne, J. C. Maan, P. C. M. Christianen, P. H. J. Kouwer, R. J. M. Nolte, H. Engelkamp, K. Blank and A. E. Rowan, *Chemical Science*, 2013, **4**, 2357.
- [35] A. W. Lees and S. F. Edwards, *J. Phys. C*, 1972, **5**, 1921.
- [36] D. R. Squire, A. C. Holt and W. G. Hoover, *Physica*, 1969, **42**, 388.